Technological Communication

BBRC Bioscience Biotechnology Research Communications

Biosc.Biotech.Res.Comm. Vol 13 (2) April-May-June 2020 Pp-875-881

Optical Properties of Bismuth Oxy Chloride (BiOCl) Using Density Functional Theory

Gagan Kant Tripathi[1], Purnima Swarup Khare[1] and K. K. Saini[2]

[1]*School of Nanotechnology (SONT) Rajiv Gandhi Proudyogiki Vishwavidyalaya (RGPV) Bhopal (M.P.) , India*

[2]*National Physical Laboratory, Dr. K.S. Krishnan Road, New Delhi-110012, India*

ABSTRACT

BiOCl Crystal's electronic band structures, density of state (DOS), and optical properties have been studied using the Local Density Approximation (LDA) density function theory. The electronic band structure obtained shows that BiOCl crystal has a forbidden band gap of 2.45 eV indirect. Using the LDA, structural optimization for BiOCl was carried out. The outcome of BiOCl's structure optimization was contrasted with the experimental findings, and it was found to be in strong agreement with these tests. It calculates the linear photon-energy-dependent dielectric functions and some optical properties, such as the function of energy-loss, the effective number of valance electrons and the effective optical dielectric constant

KEY WORDS: BIOCL, AB-INITO, BAND STRUCTURE, OPTICAL PROPERTIES.

INTRODUCTION

Bismuth oxychloride (BiOCl), a member of compounds with the general formula A= As, Sb, Bi, B= O, S, Se and X= Cl is a wide bandgap semiconductor with a tetragonal PbFCl-type structure (space group P4/nmm: No: 129) (Keramidas et al, 1993; Peng et al, 2009; Zeng et al, 2019). This crystal has 2 BiOCl molecules in a unit cell. Therefore, this compound has a complex structure with 18 valance electrons per unit cell.

The BiOCl unit cell is shown in Figure 1 (Zhang et al, 2006) and atomic positions are given in the unit cell in Table 1 (Keramidas et al, 1993). The structure of crystals can be derived from the structure of the fluorite (CaF2). The Bi atom is paired with four O atoms in one base and four Cl atoms in another. The atom O is coordinated tetrahedrally to four atoms Bi. The Cl atom is bound in a planar square with four Bi atoms to form a pyramid, with its non-bonding electrons pointing to the other side of the square. As shown in Figure 1, through the Cl atoms along the c- axis, the (BiOCl) layers are stacked together by the nonbonding (van der Waals) interaction; the structure is therefore not heavily packed in this direction (Zhang et al, 2006; Sun et al, 2019).

Within the local density approximation (LDA) by Zhang et al, 2006, the electronic structure of BiOCl was calculated using the tight-binding linear muffin-tin orbital (TB-LMTO) method (Li et al, 2018). The calculated indirect nature is in agreement with the experimentally observed linear relationship between and (where and represent, respectively, the absorption coefficient and photon energy) although the calculated band gap is

ARTICLE INFORMATION

**Corresponding Author: gagankanttripathi@gmail.com*
Received 7th April 2020 Accepted after revision 25th May 2020
Print ISSN: 0974-6455 Online ISSN: 2321-4007 CODEN: BBRCBA

Thomson Reuters ISI Web of Science Clarivate Analytics USA and Crossref Indexed Journal

NAAS Journal Score 2020 (4.31) SJIF: 2020 (7.728)

Online Contents Available at: http//www.bbrc.in/
DOI: 10.21786/bbrc/13.2/73

relatively narrow (Zhang et al, 2006; Li et al, 2017). BiOX's electronic band structure (X = F, Cl, Br, and I) was determined by Huang at al, 2009, using DFT method within GGA scheme. The atomic charges and bond orders were analyzed using the Mulliken population analysis (Mulliken, 1955; Srivastava et al, 2014; Sharma et al, 2015; Segall et al, 1996; Segall et al, 1196; Sun et al, 2018), describing the spatial distribution of orbital density (Huang at al, 2009) as well. No ab initio general possible measurements of BiOCl's optical properties have been documented in depth, as far as we know (Tripathi, 2019; Wang et al, 2019).

Table 1. Fractional atomic coordinates (Å) for BiOCl (Keramidas et al, 1993)

Atoms	x	Y	Z
Bi	0.25	0.25	0.1714(3)
O	0.25	0.75	0
Cl	0.25	0.25	0.6459(25)

Figure 1: The unit cell of BiOCl viewed along (100) (Zhang et al, 2006)

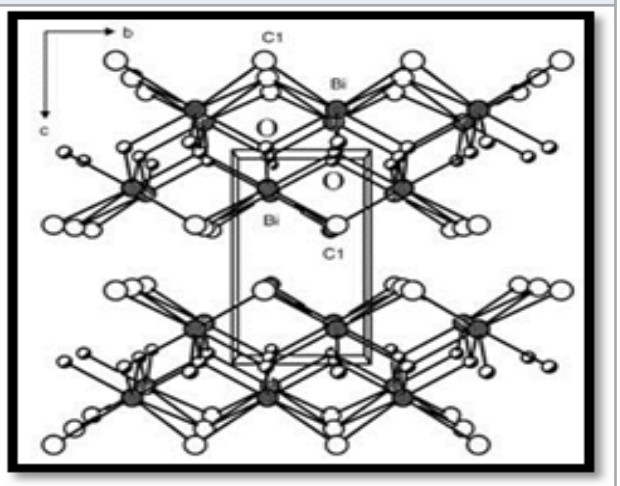

In the present work we have investigated the electronic band structure, total state density (DOS), structure optimization, and photon-energy-dependent optical properties of the BiOCl crystal using a pseudo potential approach based on the local density approximation (LDA) density functional theory (DFT) (Kohn et al, 1965; Liu et al, 2019).

MATERIAL AND METHODS

For this research, the SIESTA (Spanish Initiative for Electronic Simulations with Thousands of Atoms) code (Ordejon et al, 1996; Soler et al, 2002; Liao et al, 2020; Fitzpatrick et al, 2020) was used to measure BiOCl 's energy spectra and optical. In the LDA parameterized by Ceperley et al, 1980; it solves the quantum mechanical equation for the electron inside the DFT method. Separable Troullier et al, 1991; norm-conserving pseudopotential activates the interactions between the electrons and core ions. The basis set is based on the Sankey et al, 1989; finite range pseudoatomic orbital's (PAO's), expanded to include multiple-zeta decay (Heidari et al, 2020; Canpolat et al, 2019).

We have separately generated atomic pseudopotentials for Bi, O and Cl, using the atomic configurations $5s^2 5p^3$, $2s^2 2p^4$ and $3s^2 3p^5$, respectively. The cut-off radii are taken as 2.70, 1.15 and 1.65 a.u for current atomic pseudopotentials. For the Bi, O, and Cl channels s, p, d, and f respectively. SIESTA measures the potential of self-consistency in real space on a grid. In terms of an energy cut-off E_c, the fineness of this grid is calculated in analogy to the energy cut-off if the basis set contains plane waves. Here, we find an optimum value of around 300 R_y for BiOCl by using a double-zeta plus polarization (DZP) orbital's basis and the cut-off energies between 50 and 450 R_y with different base sets. 98 k-points for BiOCl were found to be sufficient for the final calculations to obtain the total energy with an accuracy of approximately 1 meV/atoms (Paudel et al, 2018).

RESULTS AND DISCUSSION

Structural Optimization: All physical characteristics contribute to total strength. For example, a crystal's equilibrium lattice constant is the lattice constant which minimizes total energy. If the total energy is measured, any physical property can be determined that is related to total energy. First, the equilibrium lattice parameter was determined by minimizing the total energy of the crystal determined for the different lattice constant values by means of Murnaghan's, 1994; state equation (EOS) as shown in Figure 2, and the result is shown in Table 2 along with the experimental and theoretical values. For tetragonal structures the lattice parameters for BiOCl are found to be a = b=3.88 which c=7.314, and are in good agreement with the experimental and theoretical values. We have used the computed lattice parameter in all of our calculations (Sun et al, 2019).

Figure 2: Energy versus volume curve of BiOCl

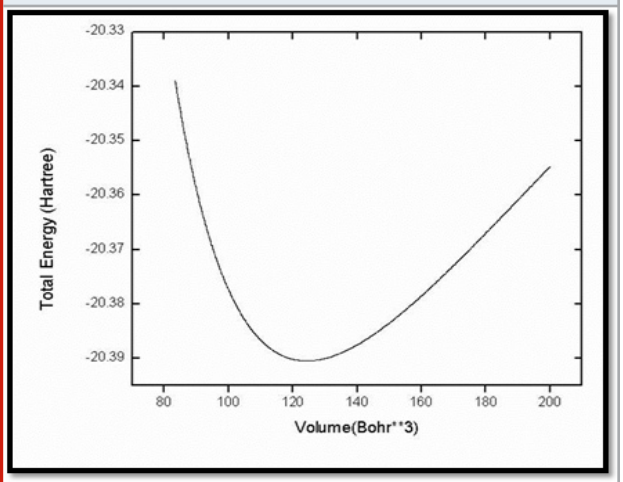

Table 2. Structure parameters of BiOCl materials

Reference	α(Å)	c (Å)	Space Group
Present	3.888	7.314	
Experimental	3.887	7.354	
Experimental	3.888	7.357	P4/nmm
Experimental	3.890	7.890	
Theory	3.824	7.243	

Electronic Band Structure: In the first Brillouin Zone (BZ) of the tetragonal system, the electronic band structures of BiOCl crystals were determined along high symmetry directions and are shown in Figure 3. The band structures were calculated along the special lines which connect the high symmetry points (1/2, 0, 0), X (1/2, 0, 0), Z (0, 0, 1/2), M (1/2, 1/2, 0), R (1/2, 0, 1/2) and A (1/2, 1/2, 1/2) in the k-space (Zhang et al, 2019).

Figure 3: First Brillouin zone for BiOCl (space group P4/nmm)

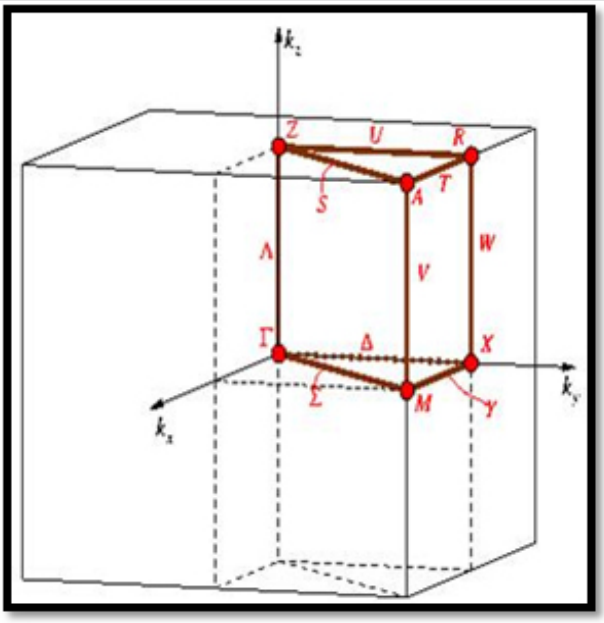

The calculation results are shown on BiOCl crystal in Figure 4. The densities of states (DOS) are shown in the rightmost panels of this Figure. Such crystals' determined band gap values are given in Table 3. In our calculations, the valance band consists of the Cl 3s and 3p states, the O atom 2s and 2p states, and the Bi atom 6s states, while the conduction band consists of the Bi atom 6p states.

Table 3. Energy band gaps for BiOCl

Referance	E_g(eV)
Present	2.45 indirect- 2.77 direct
Experimental	3.46 indirect
Theory	2.59 indirect

As can be seen in Figure 4, the top of the valance band is placed between the Z-R points near the R point and the bottom of the conductive band is located at the nearly midway point between the BZ's and Z points. Therefore the BiOCl band gap is indirect with the value 2.45 eV the lowest direct band gap value reported for BiOCl is 2.77 eV(Tripathi et al, 2017; 2016; 2015; 2016).

Figure 4: Energy band structure and DOS (density of states) for BiOCl

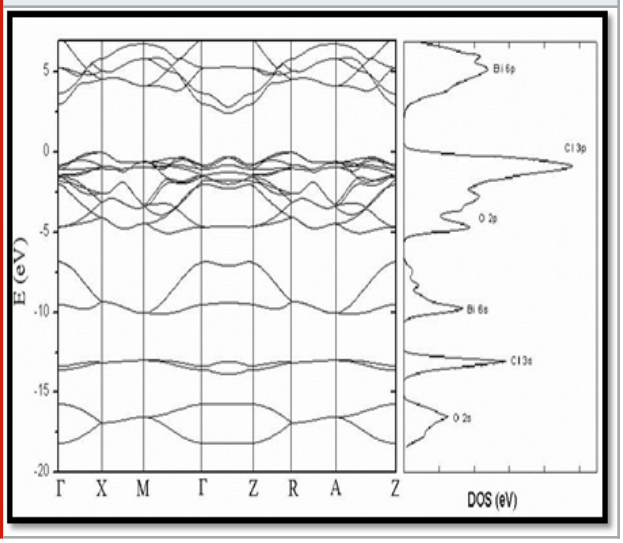

Ultimately, the values obtained for BiOCl in the band gap are less than those measured. The band gap values are underestimated than the experimental values for all of the crystal structures considered. Because of the use of pseudopotential method this is an expected case.

3.3. Optical Properties: It is well known that the effect of the electric field vector, E , of the incoming light is to polarize the material. At the level of linear response this polarization can be calculated using the following relation (Li et al, 2009; Zhang et al, 2019):

$$P^i(\omega) = \chi_j^{(1)}(-\omega,\omega)\, E^j(\omega) \quad (1)$$

Where $\chi_{ij}^{(1)}$ is the linear optical susceptibility tensor and it is given by (Levine et al, 1989)

$$\chi_{ij}^{(1)}(-\omega,\omega) = \frac{e^2}{\hbar\Omega}\sum_{m\,\vec{k}} f_m\ (\vec{k})\frac{r_m^i\ (\vec{k}) r_m^i}{\omega_m\ (\vec{k})} \quad (2)$$

Where n,m denote energy bands, $f_{mn}\ (\vec{k}) \equiv f_m(\vec{k}) - f_n(\vec{k})$ is the fermi occupation factor, Ω is the normalization volume. $\omega_{mn}\ (\vec{k}) \equiv \omega_m(\vec{k}) - \omega(\vec{k})$ are the frequency differences, $\hbar\omega_n(\vec{k})$ is the energy of band n *at* wavevector k. The $\vec{r}_{mn}$ are

are the matrix elements of the position operator and are given by

$$r^i_{nm}(\vec{k}) = \frac{v^i_{nm}(\vec{k})}{i\omega_{nm}}; \quad \omega_n \neq \omega_m \qquad \text{.....(3)}$$

$$r^i_{nm}(\vec{k}) = 0; \quad \omega_n = \omega_m$$

Where $v^i_m(\vec{k}) = m^{-1}p^i_m(\vec{k})$ m is the free electron mass, and $\vec{p}_{mn}$ is the momentum matrix element.

As can be seen from equation (2), the dielectric function $\varepsilon_j(\omega) = 1 + 4\pi\chi^{(1)}_j(-\omega,\omega)$ and the imaginary part of $\varepsilon_j(\omega)$ $\varepsilon^j_2(\omega)$ is given by

$$\varepsilon^{ij}_2(w) = \frac{e^2}{\hbar\pi}\sum_m \int d\vec{k} f_{nm}(\vec{k}) \frac{v^i_m(\vec{k}) v^j_m(\vec{k})}{\omega^2_m} \delta(\omega - \omega_m(\vec{k})). \qquad (4)$$

The real part of $\varepsilon_j(\omega)$ $\varepsilon^j_1(\omega)$ can be obtained by using the Kramers-Kroning transformation

$$\varepsilon^j_1(\omega) - 1 = \frac{2}{\pi} \wp \int_0^\infty \frac{\omega' \varepsilon^j_2(\omega')}{\omega'^2 - \omega^2} d\omega'. \qquad (5)$$

Since the Kohn-Sham equations decide the properties of the ground state, there is no physical meaning to the unoccupied conduction bands as measured. If they are used in calculating optical properties for semiconductors as single-particle states, a band gap problem is included in the response calculations. In the present work, we used the 'scissors approximation' (Levine et al, 1989; Philipp et al, 1963; Zhang et al, 2019) in order to take into account self-energy results. In the present work, , the scissor shift to make the theoretical band gap match the experimental one, is 1.01 eV for BiOCl.

Expressions for the energy-loss spectrum, $L(\omega)$.

$$L_{ij}(\omega) = -\mathrm{Im}\ \varepsilon^{-1}_j(\omega) \qquad (6)$$

The known sum rules (Kovalev, 1965) can be used to determine certain quantitative parameters, in particular the effective number of valence electrons per unit cell N_{eff}, and the effective optical dielectric constant ε_{eff} which contributes to the optical constants of an energy crystal. One can obtain an estimate of the distribution of oscillator strengths for both intra band and inter band transitions by computing the $N_{eff}(E_0)$ defined according to

$$N_{eff}(E) = \frac{2m\varepsilon_0}{\pi\hbar^2 e^2 N} \int_0^\infty \varepsilon_2(E) E dE, \qquad (7)$$

Where $N\alpha$ is the density of atoms in a crystal, e and m are the charge and mass of the electron, respectively and $N_{eff}(E_0)$ is the effective number of electrons contributing to optical transitions below an energy of (E_0)

Further information on the position of the core and semi-core bands can be obtained by measuring the contribution made by the different bands to the static dielectric constant; ε_0

According to the Kramers-Kronig relations, one has

$$\varepsilon_0(E) - 1 = \frac{2}{\pi} \int_0^\infty \varepsilon_2(E) E^{-1} dE \ . \qquad (8)$$

Thus, an 'effective' dielectric constant can be defined, which represents a different means of inter band transitions than that represented by the sum law, equation (8), depending on the relation

$$\varepsilon_{eff}(E) - 1 = \frac{2}{\pi} \int_0^{E_0} \varepsilon_2(E) E^{-1} dE \ . \qquad (9)$$

The physical meaning of ε_{eff} is quite clear: ε_{eff} is the effective optical dielectric constant governed by the inter band transitions in the energy range from zero to E0, i.e. by the polarization of the electron shells.

We have chosen a photon-energy range of 0-30 eV to calculate the optical response using the calculated band structure and have seen that a photon-energy range of 0-18 eV is sufficient for most of the optical functions.

The BiOCl crystal has an optically uniaxial, hexagonal structure. For this reason the BiOCl crystal linear dielectric tensor has two independent components that are the linear dielectric tensor's diagonal elements. Figure 5 presents the measured actual parts and imaginary parts of the linear frequency-dependent dielectric function's xx- and zz- components. The function ε_1^{xx} is equal to zero at about 6.66, 10.72, 13.90, 22.5, 22.99 and 23.23 eV (W, X, Y, Z, U and V in Figure 5), while the other function ε_1^{zz} is equal to zero at about 7.37, 8.35, 8.49, 9.90, 12.97 and 22.28 eV (W, X, Y, Z, U and V in Figure 5). The values of the ε_2^{xx} and ε_2^{zz} peaks shown in Figure 5 are summarized in Table 4. This peak corresponds to the transitions from the valance to the conduction band (see Figure 5).

The calculated energy-loss functions, $L(\omega)$, are presented in Figure 6. In this Figure, L_{xx} and L_{zz} correspond to the energy-loss functions along the x- and z- directions, respectively. The function $L(\omega)$ describes the energy loss of fast electrons traversing the material. The sharp maxima in the energy-loss function are associated with

the existence of plasma oscillations (Marton, 1956). The curves of L_{xx} and L_{zz} in Figure 6 have a maximum near 24.33 and 25.23 eV, respectively and these value coincide with the V point in Figure 5.

Table 4. Comparative characteristics of linear optical functions of BiOCl crystal

	Peaks (eV)															
ε_2	A	B	C	D	E	F	G	H	I	J	K	L	M	N	O	P
Xx	5.44	6.39	7.21	11.53	12.49	13.49	14.49	15.61	16.21	17.66	18.47	18.93	20.73	21.95	22.91	24.02
Zz	4.97	6.04	7.26	8.65	10.39	12.87	14.06	15.02	15.51	16.29	17.85	18.93	19.59	20.21	23.61	24.87

Figure 5 Energy spectra of dielectric function for BiOCl

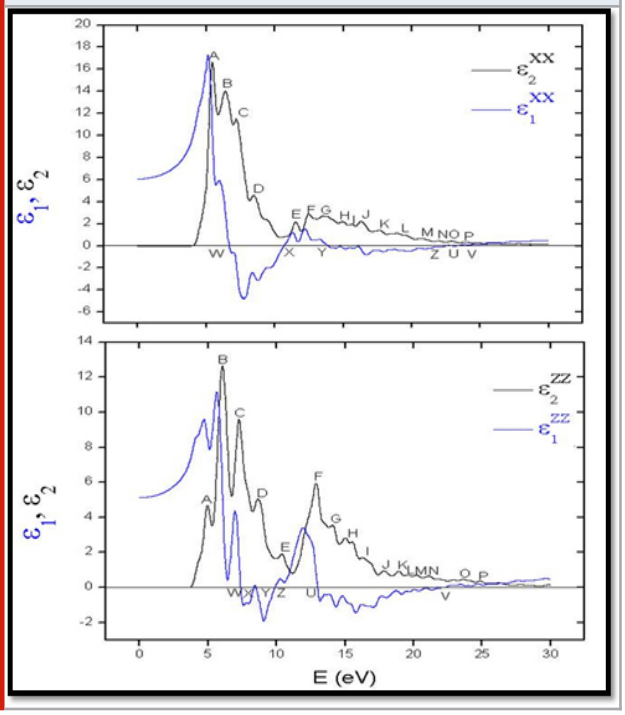

Figure 6 Energy-loss functions along the x- and z- axes for BiOCl

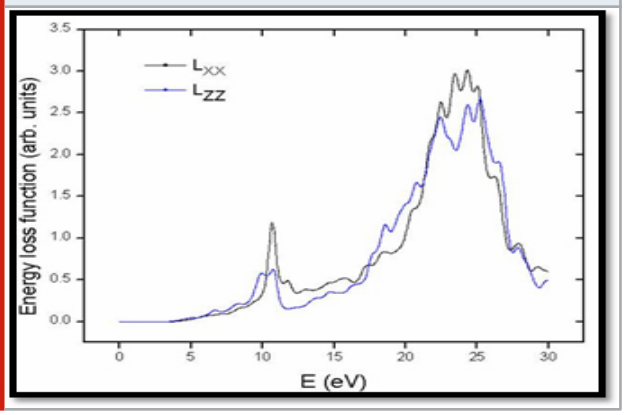

The calculated effective number of valence electrons N_{eff} and the effective dielectric constant (ε_{eff}) are given in Figure 7. The effective number of valence electron per unit cell N_{eff}, contributing in the inter band transitions, reaches saturation value at about 26 eV. This means that deep-lying valence orbital's do not participate in the inter band transitions (see Figure 4)

Figure 7: Energy spectra of and along the x- and z-axes

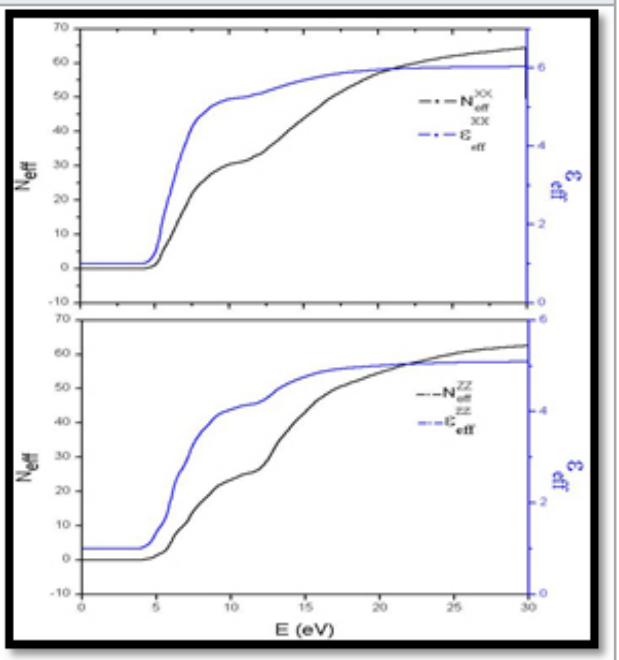

The effective optical dielectric constant ε_{eff} as shown in Figure 7, reaches a saturation value at approximately 16 eV. Dependence of the photon-energy ε_{eff} can be separated into two regions. The first is marked by a rapid rise and extends up to 10 eV. The value of ε_{eff} rises smoother and slower in the second region, and tends to saturate at 16 eV energy. This means that the greatest contribution to ε_{eff} arise from inter band transitions between 4.7 and 16 eV.

CONCLUSION

In this work we have carried out a detailed investigation of the BiOCl crystal's electronic structure and frequency-dependent linear optical properties using the density functional methods. This research had the challenge of applying the density-functional methods to a complex crystal such as the BiOCl. BiOCl crystal is seen as having the indirect forbidden gap. Our experimental results are consistent with the obtained band gap 2.45 eV values

in agreement with the previous results. The complete calculation of DOS shows that the valance band consists of 3s and 3p states of the Cl atom, 2s and 2p states of the O atom, and 6s states of the Bi atom, while the band of conduction consists of 6p states of the Bi atom. We investigated photon energy-dependent dielectric functions as well as related quantities such as power-loss ratio, the effective number of valance electrons per unit cell participating in inter band transitions and the effective optical dielectric ratio along the x- and z-axes. The results of the structural optimization carried out using the LDA are in excellent agreement with the results of the experiments.

REFERENCES

Ceperley, D.M. and Alder, B.J. (1980) Ground state of the electron gas by a stochastic method. Physical review letters, Vol. 45 No.7: Pages 566-581

Canpolat, M., Kürkçü, C., Yamçıçıer, Ç. and Merdan, Z. (2019) Structural and electronic properties of BiOF with two-dimensional layered structure under high pressure: Ab initio study. Solid State Communications, Vol. 288: Pages 33-37

Fitzpatrick, M., Rac, V.E., Mitsakakis, N., Abrahamyan, L., Pechlivanoglou, P., Chung, S., Carcone, S.M., Kendzerska, T., Zwarenstein, M., Gottschalk, R. and George, C.(2020) SIESTA-Home sleep study with BresoDx for obstructive sleep apnea: a randomized controlled trial. Sleep medicine, Vol. 65: Pages 45-53

Heidari, S., Haghighi, M. and Shabani, M. (2020) Sunlight-activated BiOCl/BiOBr–Bi24O31Br10 photocatalyst for the removal of pharmaceutical compounds. Journal of Cleaner Production, Vol. 259:Pages 120679 (1-35)

Huang, W.L. and Zhu, Q. (2009) DFT calculations on the electronic structures of BiOX (X= F, Cl, Br, I) photocatalysts with and without semicore Bi 5d states. Journal of computational chemistry, Vol. 30 No. 2: Pages183-190

Keramidas, K.G., Voutsas, G.P. and Rentzeperis, P.I. (1993) The crystal structure of BiOCl. Zeitschrift für Kristallographie-Crystalline Materials, Vol. 205: Pages 35-40

Kohn, W. and Sham, L.J. (1965) Self-consistent equations including exchange and correlation effects. Physical review, Vol. 140:, Pages 1133-1138

Kovalev, O.V. (1993) Representations of the Crystallographic Space Groups: Irreducible Representations, Induced Representations, and Corepresentations. Gordon and Breach Science

Li, L., Cao, R., Wang, Z., Li, J., and Qi, L.(2009) Template synthesis of hierarchical Bi2E3 (E=S, Se, Te) core-shell microspheres and their electrochemical and photoresponsive properties, J. Phys. Chem. C, Vol. 113: Pages 18075-18081

Levine, Z.H., and Allan, D.C.(1989) Linear optical response in silicon and germanium including self-energy effects, Phys. Rev. Lett, Vol. 63: Pages 1719-1722

Li, H., Li, J., Ai, Z., Jia, F. and Zhang, L.(2018) Oxygen vacancy-mediated photocatalysis of BiOCl: reactivity, selectivity, and perspectives. Angewandte Chemie International Edition, Vol. 57: Pages 122-138

Li, H., Qin, F., Yang, Z., Cui, X., Wang, J. and Zhang, L. (2017) New reaction pathway induced by plasmon for selective benzyl alcohol oxidation on BiOCl possessing oxygen vacancies. Journal of the American Chemical Society, Vol. 139 No. 9: Pages 3513-3521

Liu, C., Zhou, J., Su, J. and Guo, L. (2019) Turning the unwanted surface bismuth enrichment to favourable BiVO4/BiOCl heterojunction for enhanced photoelectrochemical performance. Applied Catalysis B: Environmental, Vol. 241: Pages 506-513

Liao, J., Li, K., Ma, H., Dong, F., Zeng, X. and Sun, Y. (2020) Oxygen vacancies on the BiOCl surface promoted photocatalytic complete NO oxidation via superoxide radicals. Chinese Chemical Letters (In Press)

Marton, L.(1956) Experiments on low-energy electron scattering and energy losses. Rev. Mod. Phys, Vol. 28: Pages 172-183

Murnaghan, F.D. (1944) The compressibility of media under extreme pressures. Proc. Nat. Acad. Sci. USA, Vol. 30: Pages 244-247

Mulliken,R.S. (1955) Electronic population analysis on LCAO MO molecular wave functions-I. J. Chem. Phys., Vol. 23: Pages 1833-1845

Ordejon, P., Artacho, E., and Soler, J. M. (1996) Selfconsistent order-N density-functional calculations for very large systems. Phys. Rev. B (Rapid Common), Vol. 53: Pages 10441-10444

Peng, H., Chan, C.K., Meister, S.M., Zhang, X.F., and Cui,Y. (2009) Shape evolution of layer-structured bismuth oxychloride nanostructures via low-temperature chemical vapor transport. Chem. Mater, Vol. 21: Pages 247-252

Philipp, H., and Ehrenreich, RH. (1963) Optical properties of semiconductors. Phys. Rev., Vol. 129: Pages 1550-1560

Paudel, S., Adhikari, P.R., Upadhyay, O.P., Kaphle, G.C. and Srivastava, A. (2018) First Principles Study of Electronic and Optical Properties of Pristine and X (Cu, Ag And Au) Doped BiOBr. Journal of Institute of Science and Technology, Vol. 22: Pages 63-69

Sun, H., Tian, Z., Zhou, G., Zhang, J. and Li, P. (2019) Exploring the effects of crystal facet in Bi2WO6/BiOCl heterostructures on photocatalytic properties: A first-principles theoretical study. Applied Surface Science, Vol. 469: Pages 125-134

Sun, J., Wu, S., Yang, S.Z., Li, Q., Xiong, J., Yang, Z., Gu, L., Zhang, X. and Sun, L. (2018) Enhanced photocatalytic activity induced by sp3 to sp2 transition of carbon dopants in BiOCl crystals. Applied Catalysis

B: Environmental, Vol. 221: Pages 467-472

Sun, X., Wang, M., Qian, N.X., Sun, X.Y., Liu, C., Zhang, X., Rao, R. and Ma, Y.Q. (2019) Ultra-fine BiOCl nanoparticles: Unprecedented synthesis and rich surface-dependent properties. Applied Surface Science, Vol. 489: Pages 1030-1041

Sankey, O.F., and Niklewski, D.J. (1989) Ab initio multicenter tight-binding model for molecular-dynamics simulations and other applications in covalent systems. Phys. Rev B, Vol. 40: Pages 3979-3995

Soler, J.M., Artaeho, E., Gole, J.D., Garsia, A., Ordejon, J. P., and Sanchez-portal, D. (2002) The SIESTA method for ab initio order-N materials simulation. J. Phys: Condens Matter, Vol. 14: Pages 2745-2779

Segall, M.D., Shah, R., Pickard, C.J., and Payne,M.C. (1996) Population analysis of plane wave electronic structure calculations of bulk materials. Phys. Rev. B, Vol. 54: Pages 16317-16320,

Segall, M.D., Pickard, C.J., Shah, R., and Payne, M.C. (1996) Population analysis in plane wave electronic structure calculations. Mol. Phys., Vol. 89: Pages 571

Sharma, I.D., Tripathi, G.K., Sharma, V.K., Tripathi, S.N., Kurchania, R., Kant, C., Sharma, A.K. and Saini, K.K. (2015) One-pot synthesis of three bismuth oxyhalides (BiOCl, BiOBr, BiOI) and their photocatalytic properties in three different exposure conditions. Cog. Chemi., Vol. 1: Pages 1076371(1-15)

Srivastava, P., Jaiswal, N.K. and Tripathi, G.K. (2014) Chlorine sensing properties of zigzag boron nitride nanoribbons. Sol. Stat. Comm., Vol. 185: Pages 41-46

Troullier, N. J., and Martins, L. (1991) Efficient pseudopotentials for plane-wave calculations. Phys. Rev. B, Vol. 43: Pages 1993-2006

Tripathi, G.K. and Kurchania, R. (2017) Photocatalytic behavior of BiOX (X= Cl/Br, Cl/I and Br/I) composites/ heterogeneous nanostructures with organic dye. Opt. and Quan. Elect., Vol. 49: Pages 203-211

Tripathi, G.K., Sharma, I.D., Kant, C., Pandey, R.R., Saini, K.K. and Kurchania, R. (2016) Characterization of the photocatalytic activity of bismuth oxychloride nanostructures. Analy. Lett., Vol. 49: Pages 1452-1466

Tripathi, G.K., Saini, K.K. and Kurchania, R. (2015) Synthesis of nanoplate bismuth oxychloride-a visible light active material. Opt. and Spect., Vol. 119: Pages 656-663

Tripathi, G.K. and Kurchania, R. (2016) Effect of doping on structural, optical and photocatalytic properties of bismuth oxychloride nanomaterials. J. of Mater. Scie.: Mate. in Elec., Vo. 27: Pages 5079-5088

Tripathi, G.K. (2019) Engineered Nanomaterials and Their Properties: A Review. Biosci. Biotech. Res. Comm., Vol. 12 No. 3: Pages 764-771

Wang, J., Wei, Y., Yang, B., Wang, B., Chen, J. and Jing, H. (2019) In situ grown heterojunction of Bi2WO6/ BiOCl for efficient photoelectrocatalytic CO2 reduction. Journal of Catalysis, Vol. 377: Pages 209-217

Zhang, K.-L., Liu, C.-M., Huang, F.-Q., Zheng, C., and Wang, W.-D. (2006) Study of the electronic structure and photocatalytic activity of the BiOCl photocatalyst. Applied Catalysis B: Environmental, Vol. 68: Pages 125-129

Zeng, R., Luo, Z., Su, L., Zhang, L., Tang, D., Niessner, R., & Knopp, D. (2019) Palindromic molecular beacon based Z-scheme BiOCl-Au-CdS photoelectrochemical biodetection. Analytical chemistry, Vol. 91: Pages 2447-2454

Zhang, H., Alameen, A., An, X., Shen, Q., Chang, L., Ding, S., Du, X., Ma, X., Hao, X. and Peng, C. (2019) Theoretical and experimental investigations of BiOCl for electrochemical adsorption of cesium ions. Physical Chemistry Chemical Physics, Vol. 21: Pages 20901-20908